

VersaViT: Enhancing MLLM Vision Backbones via Task-Guided Optimization

Yikun Liu^{1,2*}, Yuan Liu^{3†}, Shangzhe Di^{1,2}, Haicheng Wang^{1,2}, Zhongyin Zhao³, Le Tian³, Xiao Zhou³, Jie Zhou³, Jiangchao Yao², Yanfeng Wang^{1†}, Weidi Xie¹

¹School of Artificial Intelligence, Shanghai Jiao Tong University, China
²CMIC, Shanghai Jiao Tong University, China ³ WeChat AI, Tencent Inc., China

Abstract

Multimodal Large Language Models (MLLMs) have recently achieved remarkable success in visual-language understanding, demonstrating superior high-level semantic alignment within their vision encoders. An important question thus arises: Can these encoders serve as versatile vision backbones, capable of reliably performing classic vision-centric tasks as well? To address the question, we make the following contributions: (i) we identify that the vision encoders within MLLMs exhibit deficiencies in their dense feature representations, as evidenced by their suboptimal performance on dense prediction tasks (e.g., semantic segmentation, depth estimation); (ii) we propose VersaViT, a well-rounded vision transformer that instantiates a novel multi-task framework for collaborative post-training. This framework facilitates the optimization of the vision backbone via lightweight task heads with multi-granularity supervision; (iii) extensive experiments across various downstream tasks demonstrate the effectiveness of our method, yielding a versatile vision backbone suited for both language-mediated reasoning and pixel-level understanding. The project page is available [here](#).

1. Introduction

Multimodal large language models (MLLMs) have emerged as the prevailing paradigm for vision-language understanding [1, 13, 21, 59]. Architecturally, contemporary MLLMs consist of a vision encoder, a vision-language projection module, and a large language model (LLM). Among these, the vision encoder plays a pivotal role in linking visual perception with language reasoning. In practice, it is commonly initialized from CLIP-style encoders [50, 62] trained with contrastive learning [47], and then jointly optimized with the LLM via instruction tuning on large-scale visual question answering (VQA) and captioning corpora. This

*Work was done during internship in WeChat.

†Corresponding author.

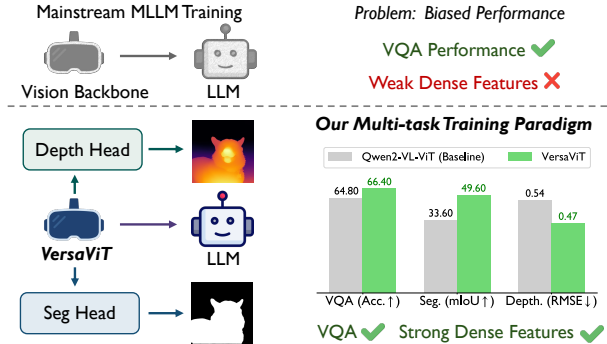


Figure 1. **Overcoming the dense feature limitation of vision backbone within MLLMs.** We observe the vision encoder within MLLMs (Top), which yields strong VQA but suboptimal dense features. Conversely, our multi-task collaborative post-training (Bottom) is designed to overcome this limitation by comprehensively enhancing the vision encoder’s capabilities.

pipeline has yielded state-of-the-art results on a broad spectrum of visual-language understanding tasks.

Despite the excellent performance on instruction following and open-ended VQA [1, 21, 39, 73], it remains unclear whether MLLM vision encoders retain the pixel-level perception and spatial precision, that are often required for classic vision-centric problems, for example, segmentation, depth estimation. This question is central if we aim to evolve these encoders into true vision foundation models (VFs) that are equally competent at language reasoning and pixel-level perception. To probe this, we conduct linear probing on monocular depth estimation and semantic segmentation using the vision backbones of the Qwen-VL series [1, 68]. Our initial results (Section 3) reveal notable deficiencies on dense prediction benchmarks, suggesting a representational misalignment: pretraining and instruction tuning emphasize global semantic alignment and language grounding, but do not sufficiently regularize the fine-grained visual features critical for dense tasks.

This observation motivates our central question: *can we adapt MLLM vision encoders so that they simultaneously excel at vision-language reasoning and vision-centric dense prediction, yielding a genuinely well-rounded vision*

foundation model ? We posit that the gap arises less from architectural limits and more from the training curriculum and supervision granularity. Specifically, contrastive pretraining followed by text-centric instruction tuning provides limited multi-scale spatial supervision and sparse pixel-level signals, which can erode fine-grained dense representation.

To this end, we introduce **VersaViT**, a well-rounded vision transformer obtained by post-training the vision encoder of existing MLLMs with multi-granularity supervision and lightweight task-specific heads. Our framework couples the shared backbone with auxiliary heads to (i) expose the encoder to complementary signals spanning high-level semantics, mid-level spatial reasoning, and pixel-level perception, while (ii) isolating task-specific conflicts in the heads rather than in the shared representation. Concretely, we instantiate three representative supervision families: (1) VQA and image captioning for semantic grounding and instruction-following, (2) monocular depth estimation for 3D-aware spatial structure, and (3) referring image segmentation for localized, language-conditioned pixel precision. This framework jointly optimizes the backbone and all auxiliary heads with a simple multi-task objective, biasing the shared representation toward transferable, dense-friendly features without sacrificing language grounding.

We validate VersaViT across a wide range of downstream tasks, including VQA, semantic segmentation, referring segmentation, monocular depth estimation, and image–text retrieval. Empirically, VersaViT improves VQA performance while substantially strengthening dense prediction accuracy, indicating that multi-granularity signals can be synergistic rather than competitive when mediated by lightweight heads. Moreover, our framework is modular and aligns with MLLM training pipelines, enabling drop-in integration with minimal engineering overhead.

In summary, we make the following contribution: (i) diagnosis. We identify a consistent shortfall in dense representations of mainstream MLLM vision encoders, manifested by underperformance on depth and segmentation under linear probing; (ii) method. We propose VersaViT, a well-rounded vision transformer that instantiates a multi-task collaborative post-training framework. This framework augments an MLLM vision encoder with lightweight auxiliary heads for VQA/captioning, depth estimation, and referring segmentation, delivering multi-granularity supervision to the shared backbone; (iii) evidence. Extensive experiments show that VersaViT simultaneously advances VQA and dense prediction, yielding a more balanced, transferable vision backbone suited for both language-mediated reasoning and pixel-level understanding.

2. Related Work

Vision Foundation Models. Developing a robust foundation model for computer vision remains a fundamen-

tal challenge within the field. Various approaches have been adopted to advance the development of vision foundation models, which can be broadly categorized into two scalable learning paradigms: self-supervised and weakly-supervised learning. Recent self-supervised methods, including MAE [22], iBOT [90], and the DINO series [6, 48, 57], mainly use large-scale curated image datasets to construct suitable proxy tasks for learning generalizable visual representations. In contrast, weakly-supervised learning leverages web-scale image-text pairs for training. This paradigm includes models such as CLIP [50], ALIGN [25], and SigLIP [86], which utilize contrastive learning [47], as well as more recent models like CapPa [61], LocCa [64] and OpenVision2 [40], together with the Qwen-VL series [1, 68] and other MLLMs [21, 59, 77, 82], which rely on autoregressive loss for training from scratch or for fine-tuning the vision encoder to achieve improved visual representations. In this paper, we focus on enhancing the representation capability of vision encoders within MLLMs through task-guided post-training optimization.

Multimodal Large Language Models. With recent advancements in LLMs [5, 26, 60], increasing attention has been directed toward MLLMs, which aim to align visual and textual modalities via visual instruction tuning. Recent studies [1, 21, 59, 66, 68] either seek to enhance the performance of MLLMs across various VQA benchmarks by improving data scaling and selection, architectural design, and training strategies, or leverage the powerful capabilities of MLLMs to repurpose them for other visual-language tasks [32, 33, 41, 65], such as multimodal retrieval, temporal grounding, and image referring segmentation. However, the intrinsic quality and characteristics of the visual features learned by the MLLM’s vision encoder remain largely unexplored and unaddressed. Therefore, we aim to investigate this critical issue and further leverage these insights to enhance the vision encoder’s representation.

Multi-task Learning. Multi-task learning [7, 12, 14, 63, 75, 78, 91] enables models to generalize across diverse tasks, fostering the development of versatile systems that no longer rely on task-specific architectures. In natural language processing (NLP), this paradigm has been successfully realized by framing a wide range of text-related tasks within a sequence-to-sequence formulation, which has facilitated the emergence of LLMs [5, 60]. Inspired by this paradigm, the multimodal domain has also witnessed a surge of research on unified multimodal models [23, 53, 67, 71, 76]. These approaches typically reformulate multimodal tasks, which span from image captioning to visual question answering, as sequence-to-sequence problems or leverage LLMs as bridges to connect different task heads. Motivated by these developments, we explore the joint training of multiple vision tasks to enhance the vision backbone.

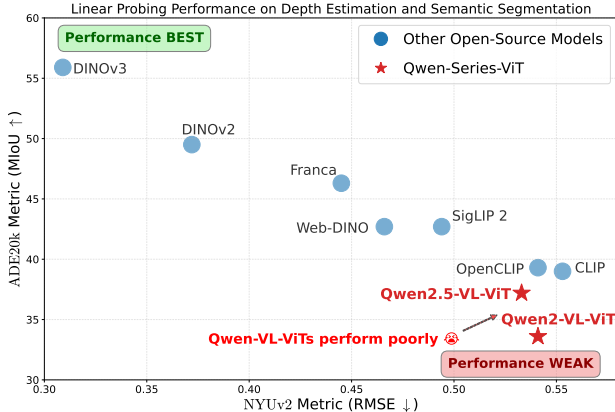


Figure 2. **Linear probing performance on depth estimation (NYUv2) and semantic segmentation (ADE20k) across different vision backbones.** The results reveal that the qwen-vl-vits exhibit suboptimal performance on these vision-centric benchmarks.

3. Motivation

Recent vision encoders developed within the MLLM paradigm have demonstrated exceptional proficiency in handling VQA tasks. However, a practical vision foundation model (VFM) should be broadly useful beyond dialog, supporting perception systems that require spatial precision, geometric consistency, and pixel-level fidelity. This raises a critical question: *Are current MLLM vision encoders effective VFMs, or do they exhibit systematic gaps when applied to classic vision-centric tasks?* To explore this, we conduct a linear probing evaluation, assessing two representative encoders, Qwen2-VL-ViT [68] and Qwen2.5-VL-ViT [1], on monocular depth estimation and semantic segmentation. As shown in Figure 2, both encoders underperform substantially in this setting. These results suggest a representational skew induced by the prevailing training recipe, which prioritizes global semantic alignment while under-regularizing intermediate and fine-grained visual structures.

Guided by these findings, we ask: Can MLLM encoders be rebalanced toward dense-friendly features without sacrificing their language grounding via low-cost post-training? Our hypothesis is that multi-granularity supervision, combining high-level semantic grounding (VQA/captioning), mid-level spatial reasoning (*e.g.*, depth estimation), and pixel-level localization (*e.g.*, referring segmentation), can remedy the observed skew with minimal architectural change. We implement this idea in VersaViT, which is optimized via a collaborative multi-task post-training framework that attaches lightweight, task-specific heads to a shared vision backbone. The heads provide task-targeted gradients and absorb conflicts, while the vision backbone is nudged toward representations that are both instruction-competent and dense-friendly. This design intentionally prioritizes practicality: it is modular, compatible with standard MLLM pipelines, and avoids full-scale retraining.

In summary, our motivation is empirical and application-driven: current MLLM vision encoders fail to reliably apply to dense prediction tasks, despite excelling at VQA. We show that a low-cost, multi-granularity post-training can close this gap, yielding a more balanced and useful VFM.

4. Method

This section starts by formulating our considered problem in Section 4.1; then we elaborate on the overall multi-task collaborative post-training framework in Section 4.2; lastly, we detail the training strategy of VersaViT in Section 4.3.

4.1. Problem Formulation

Our goal is to strengthen the MLLM vision backbone so that its representations support both language-mediated reasoning and dense, pixel-level perception. To this end, we propose VersaViT, a well-rounded vision backbone that is optimized by a multi-task collaborative post-training framework. This framework augments a shared vision encoder with lightweight, task-specific heads, enabling multi-granularity supervision with minimal architectural change. As shown in Figure 3, we select three representative tasks: (i) VQA and image captioning for semantic alignment with language, (ii) monocular depth estimation for 3D-aware spatial reasoning, and (iii) image referring segmentation for localized, language-conditioned perception.

Our framework uses separate data streams for each task. To simplify, we illustrate this using a single image for all tasks. Given an input image $\mathbf{I} \in \mathbb{R}^{H \times W \times 3}$, the shared vision encoder (Φ_V , parameterized by θ_V) first extracts the corresponding visual features ($\{\mathcal{F}_i^V\}_{i=1}^N$), where N denotes the number of the transformer layers within the vision encoder. The extracted features are subsequently routed to task-specific heads with parameters θ_{heads} . The resulting respective task losses (\mathcal{L}_{cap} , $\mathcal{L}_{\text{depth}}$, \mathcal{L}_{seg}) are aggregated to form a combined objective \mathcal{L}_{all} , which is backpropagated to collaboratively optimize and strengthen the shared vision backbone (Φ_V) across all objectives. The overall optimization goal is to find the optimal parameters for both the backbone and the heads by minimizing the combined loss:

$$\min_{\theta_V, \theta_{\text{heads}}} \mathcal{L}_{\text{all}} = \sum_{\tau \in \mathcal{T}} \lambda_{\tau} \mathcal{L}_{\tau}(\theta_V, \theta_{\tau}),$$

where $\mathcal{T} = \{\text{cap}, \text{depth}, \text{seg}\}$ is the set of all tasks, λ_{τ} is the task weight hyperparameter, and θ_{τ} represents the parameters for the head of task τ .

4.2. Overall Framework

In this section, we provide a detailed breakdown of our proposed multi-task collaborative training framework by successively introducing the three auxiliary training tasks: VQA and image captioning, monocular depth estimation, and image referring segmentation.

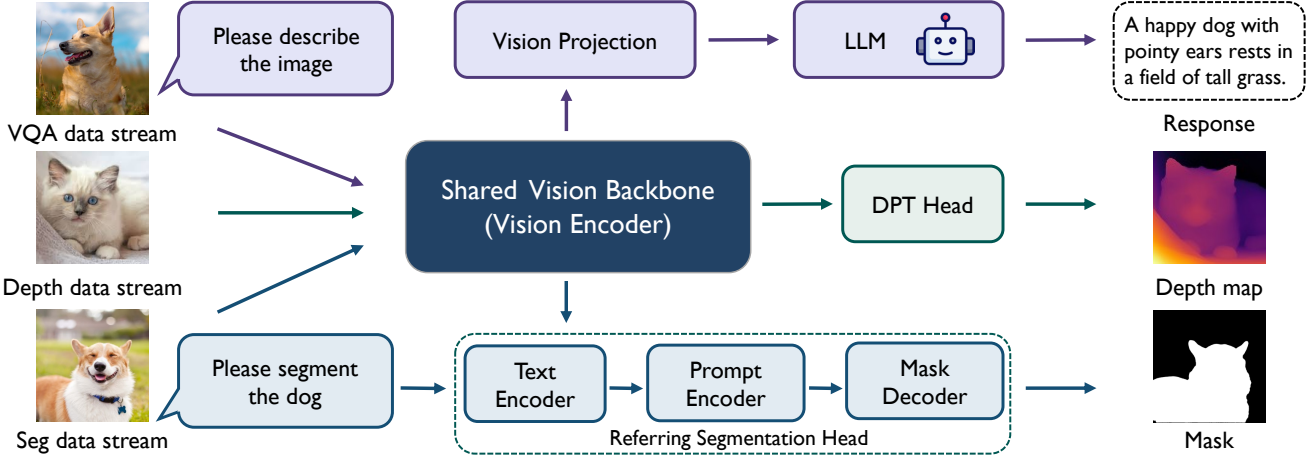


Figure 3. **Overview of the proposed multi-task collaborative training framework.** The proposed framework jointly trains three distinct tasks: VQA and Image Captioning, Monocular Depth Estimation, and Image Referring Segmentation. By incorporating lightweight task heads, this collaborative training strategy is designed to enhance the representational capabilities of the underlying vision backbone.

4.2.1. Generative Vision-Language Fine-Tuning

To enhance the high-level semantic understanding of the vision backbone, the combined VQA and image captioning tasks are integrated. This section details the components and training for the VQA&image captioning tasks.

Core Components. To accomplish the tasks of VQA and image captioning, we adopt the mainstream MLLM architecture [36]. Specifically, our main components consist of a vision encoder (Qwen2-VL-ViT), a vision projector (an MLP Layer), and a large language model (Qwen3-1.7B).

Training Pipeline. For the VQA and image captioning task, we utilize the final layer feature (\mathcal{F}_N^V) from the vision encoder. Given an input image I and an associated text $t = (t_0, t_1, \dots, t_L)$ with the token length of L , the visual feature (\mathcal{F}_N^V) is first passed through a vision projector to obtain the projected image embeddings. These projected image embeddings are then concatenated with the input text embedding derived from t via a text embedding layer. The resulting sequence forms the full input for the LLMs. The training objective are as follows: $\mathcal{L}_{\text{cap}} = \frac{1}{L} \sum_{i=1}^L \mathcal{L}_{\text{ce}}(t_i | I, t_0, \dots, t_{i-1})$.

Captioning Alignment Warm-Up. Prior to the multi-task collaborative training phase, we employ the captioning task to warm up the vision projection. Crucially, during this stage, both the vision backbone and the LLM are frozen; we exclusively train the vision projection using autoregressive loss (\mathcal{L}_{cap}). For training data, we incorporate a variety of sources, including natural image-text pairs (e.g., pixmocap [13] and SA-1B-InternVL [30]) and optical character recognition (OCR) data (e.g., idl-wds [3]).

4.2.2. Monocular Depth Estimation

To address the feature deficiency in spatial awareness and improve geometric representation, the monocular depth es-

timation task is incorporated. This section introduces the methodology for obtaining the depth prediction and corresponding pseudo ground truth label for model training, as well as the training objective employed.

Depth Prediction. For monocular depth estimation, we select a uniform subset of features from the extracted visual features ($\{\mathcal{F}_i^V\}_{i=1}^N$). Specifically, we uniformly sample three of these features and feed them into a DPT head [52] to generate the final depth prediction ($d^* \in \mathbb{R}^{H \times W}$).

Pseudo Depth Labeling. We do not rely on manually annotated ground truth data. Instead, we employ a pseudo-labeling strategy to generate the depth labels. Specifically, we adopt the Depth Anything V2 model [79] to annotate the images to get the depth labels ($d \in \mathbb{R}^{H \times W}$). Details regarding the data sources are provided in Table 1.

Training Objective. We use a scale- and shift-invariant loss \mathcal{L}_{ssi} and a gradient matching loss \mathcal{L}_{gm} to optimize depth estimation. Specifically, $\mathcal{L}_{\text{ssi}} = \frac{1}{HW} \sum_{i=1}^{HW} \rho(d_i^*, d_i)$, where ρ is the affine-invariant mean absolute error loss. \mathcal{L}_{gm} evaluate the gradient difference between the ground truth and the rescaled estimates on multiple scales k :

$$\mathcal{L}_{\text{gm}} = \sum_{k=1}^K \sum_{i=1}^{HW} |s \nabla_x^k d_i - \nabla_x^k d_i^*| + |s \nabla_y^k d_i - \nabla_y^k d_i^*|.$$

The final loss function is given by: $\mathcal{L}_{\text{depth}} = \lambda_{\text{ssi}} \mathcal{L}_{\text{ssi}} + \lambda_{\text{gm}} \mathcal{L}_{\text{gm}}$, where λ_{ssi} and λ_{gm} are weight hyperparameters. Please refer to the supplementary materials for more details.

4.2.3. Image Referring Segmentation

To instill robust localization and pixel-level fine-grained perception into the visual representation, the image referring segmentation task is employed. This section outlines the way to get the mask prediction, the data scaling strategy, and the corresponding training objective.

Mask Prediction. Given an input image I and an associated text prompt t , we use the final layer feature (\mathcal{F}_N^V) from the vision encoder. Subsequently, we utilize a pretrained text embedding model (Qwen3-Embedding-8B [87]) as the text encoder to offline extract the corresponding text embedding. Furthermore, this text embedding is then processed by the prompt encoder to yield the prompt embedding (\mathcal{F}^P). Ultimately, the mask decoder efficiently mapping \mathcal{F}_N^V , \mathcal{F}^P , and an output token to generate the final mask (\hat{M}). For further details about the architecture of the prompt encoder and mask decoder, please refer to [30].

Segmentation Data Construction. To efficiently scale the segmentation data, which is structured as an image I associated with a set of P instance-level pairs $\{(t_i, M_i)\}_{i=1}^P$ (where t_i is the text description and M_i is the corresponding mask), we employ the following three strategies: (i) We directly integrate existing referring segmentation datasets. (ii) For datasets already possessing mask annotations (e.g., SA-1B), we leverage a dense captioning model (e.g., Describe Anything [34]) to generate a text annotation for each mask. (iii) For datasets annotated only with bounding boxes and class labels, we first use SAM [30] to generate precise masks based on the bounding boxes, and subsequently apply the Describe Anything or the existing class label for text description annotation. For detailed data regarding segmentation, please refer to Table 1.

Training Objective. We utilize a combination of per-pixel binary cross-entropy (BCE) loss and DICE loss, with corresponding loss weights λ_{bce} and λ_{dice} . Given the ground-truth target masks (M), the overall loss is formulated as $\mathcal{L}_{\text{seg}} = \lambda_{\text{bce}} \mathcal{L}_{\text{bce}}(\hat{M}, M) + \lambda_{\text{dice}} \mathcal{L}_{\text{dice}}(\hat{M}, M)$.

4.3. Model Training

In this section, we describe the details of our multi-task collaborative training, which uses diverse multi-task objectives to advance the capabilities of the vision backbone.

Multi-task Collaborative Training. After captioning alignment, we adopt the multi-task collaborative training schema involving the three objectives detailed in Section 4.2: VQA&captioning (\mathcal{L}_{cap}), monocular depth estimation ($\mathcal{L}_{\text{depth}}$), and image referring segmentation (\mathcal{L}_{seg}). During this phase of training, the weights of the vision encoder, the task-specific heads, and the LLM are all unfrozen and updated. We perform joint optimization via alternating batch sampling combined with gradient accumulation. Specifically, we alternately sample a batch of data from each of the three tasks for a forward pass. The loss of each task is used to compute and accumulate gradients, with the collective parameter update executed after iterating through all three tasks. The final loss is a weighted sum:

$$\mathcal{L}_{\text{all}} = \lambda_{\text{cap}} \mathcal{L}_{\text{cap}} + \lambda_{\text{depth}} \mathcal{L}_{\text{depth}} + \lambda_{\text{seg}} \mathcal{L}_{\text{seg}},$$

where λ_{cap} , λ_{depth} and λ_{seg} are weight hyperparameters.

Table 1. **Statistics of the training data.** This table summarizes the datasets utilized in our model training.

Training Stage	Task	Data Source	Data Size
Captioning Alignment	Image Captioning	Pixmo-cap [13]	0.6M
		IDL-WDS [3]	4.7M
		SA-1B-InternVL [30]	4.1M
Multi-task Collaborative Training	Depth Estimation	Open-images [31]	1.7M
		Objects365 [55]	1.7M
		Google-landmark [69]	2.7M
	Referring Segmentation	Places365 [89]	8.0M
		SA-1B [30]	11.0M
		CC3M [8]	2.8M
VQA&Image Captioning	FineVision [70]	GRIT [49]	13.9M
		Objects365 [55]	1.6M
		SA-1B-DAM [34]	0.6M

Jointly optimizing these objectives enables the vision backbone to capture high-level semantics and strengthen pixel-level and spatial-aware representations.

5. Experiments

5.1. Experimental Setup

Training Datasets. Our training is supported by a diverse dataset spanning varied sources. Specifically, the captioning alignment stage primarily utilizes high-quality image-caption and OCR data. Subsequently, during the multi-task collaborative training phase, we either collect or synthesize new data tailored to each respective task. The comprehensive details of the training data are presented in Table 1.

Evaluation Settings. To comprehensively assess the performance of VersaViT, we conduct evaluations across multiple downstream tasks. (i) VQA performance: To evaluate VersaViT’s performance on VQA, we adopt an MLLM evaluation strategy. Specifically, we integrate VersaViT with a vision projection layer and an LLM (Qwen3-8B). The training is performed in two stages: in the first stage, only the vision projection layer is trained; in the second stage, both the vision projection layer and the LLM are trained. Throughout this entire training process, the parameters of the vision encoder are kept frozen. For details regarding the training data utilized for VQA evaluation, please refer to the supplementary materials. (ii) Dense Feature Probing: To demonstrate VersaViT’s capability for dense feature representation, we follow the methodology of [57] by employing a linear probing approach with the vision backbone kept frozen. (iii) In-Task and Out-of-Task Performance: To assess our model’s performance on the tasks included in the multi-task collaborative training stage, we conduct evaluations using established benchmarks specific to those tasks and compare the results against specialized models. Furthermore, for out-of-task generalization, we evaluate VersaViT’s retrieval performance on corresponding benchmarks.

Table 2. **Comparison between different methods on OpenCompass benchmarks, a collection of eight general VQA benchmarks.** We assess our method on the following benchmarks, MMBench [38], MMstar [10], MMMU [85], MathVista [43], HallusionBench [19], AI2D [29], OCRBench [37], MMVet [83]. For details on our VQA training and data, please refer to the supplementary materials.

Method	MMBench	MMStar	MMMU	MathVista	HallusionBench	AI2D	OCRBench	MMVet	Avg.
Open-Source Models (without access to the training data)									
MiniCPM-V-2.6 [81]	78.0	57.5	49.8	60.8	48.1	82.1	85.2	60.0	65.2
DeepSeek-VL2 [72]	81.2	61.9	54.0	63.9	45.3	83.8	80.9	60.0	66.4
Qwen2-VL-7B [68]	81.0	60.7	53.7	61.6	50.4	83.0	84.3	61.8	67.1
Qwen2.5-VL-7B [1]	82.2	64.1	58.0	68.1	51.9	84.3	88.8	69.7	70.9
Ours (LLM = Qwen3-8B)									
Qwen2-VL-ViT [68]	78.2	59.3	51.0	62.1	49.0	79.4	80.6	58.7	64.8
	78.0	60.9	53.1	63.7	51.3	79.1	82.2	62.6	66.4
VersaViT	(-0.2)	(+1.6)	(+2.1)	(+1.6)	(+2.3)	(-0.3)	(+1.6)	(+3.9)	(+1.6)

Table 3. **Linear probing results on semantic segmentation and monocular depth estimation with frozen backbones.** We report the mean Intersection-over-Union (mIoU) metric for ADE20k, Cityscapes, and VOC. We report the Root Mean Squared Error (RMSE) metric for the depth benchmarks NYUv2 and KITTI. For segmentation, we use an image resolution of 560×560 .

Method	Arch.	Segmentation		Depth		NYUv2 ↓	KITTI ↓
		ADE20k	Citysc.	VOC	NYUv2 ↓		
Self-supervised Backbone							
MAE [22]	H/14	33.3	58.4	67.6	0.517	3.660	
Web-DINO [17]	7B/14	42.7	68.3	76.1	0.466	3.158	
DINOv3 [57]	7B/16	55.9	81.1	86.6	0.309	2.346	
Weakly-supervised Backbone							
OpenCLIP [11]	G/14	39.3	60.3	71.4	0.541	3.570	
SigLIP 2 [62]	G/16	42.7	64.8	72.7	0.494	3.273	
PEcore [4]	G/14	38.9	61.1	69.2	0.590	4.119	
Ours							
Qwen2-VL-ViT [68]	H/14	33.6	57.6	67.5	0.541	3.735	
		49.6	74.5	86.6	0.473	3.136	
VersaViT	H/14	(+16.0)	(+16.9)	(+19.1)	(-0.068)	(-0.599)	

Implementation Details. Our framework is built on PyTorch and is initialized by Qwen2-VL-7B-ViT [68]. Our model is capable of accepting dynamic resolutions. In the captioning alignment stage, we conduct experiments on 128 H20 GPUs with a batch size of 1024 and a learning rate of 1e-3, training for one epoch. During the multi-task collaborative training phase, the learning rate for the vision encoder, the vision projection, and the text decoder is set to 1e-5, while the learning rate for the remaining parameters is set to 1e-4, again for one epoch. For more implementation details, please refer to the supplementary materials.

5.2. Experimental Results

In this section, we compare VersaViT with the Qwen2-VL-ViT baseline across both VQA and classic vision-centric tasks to demonstrate the effectiveness of our method.

Improved VQA Performance. As outlined in Section 5.1, we adopt a two-stage training paradigm based on MLLMs

Table 4. **Ablation study on multi-task training.** Here, we report the average score on the OpenCompass, the RMSE on the NYUv2, and the MIoU on the ADE20k.

VQA&Cap.	Depth	Seg	OpenCompass↑	NYUv2↓	ADE20k↑
✗	✗	✗	64.8	0.541	33.6
✓	✗	✗	66.1	0.557	32.0
✓	✓	✗	66.3	0.495	35.1
✓	✓	✓	66.4	0.473	49.6

to evaluate our vision backbone on various VQA tasks. Table 2 presents the performance of our model on the OpenCompass benchmark. The results indicate that (i) Crucially, under a fair comparison setting, our model demonstrates a significant improvement over the Qwen2-VL-ViT [68] baseline, achieving an average gain of 1.6 points across eight benchmarks. This consistent gain strongly suggests that our backbone’s high-level semantic representations are superior to the baseline. (ii) When VersaViT is coupled with an LLM through instruction tuning with small-scale data, it generally outperforms several well-established open-source models, such as MiniCPM-V-2.6 [81] and DeepSeek-VL2 [72]. However, a performance gap remains when compared to top-tier MLLMs, such as Qwen2.5-VL-7B [1], primarily due to differences in data scale. For further details regarding the data and training for these two stages, please refer to the supplementary materials.

Improved Dense Features. To evaluate the dense features of our method, we utilize the frozen patch features from the final layer and assess their performance through linear probing on both semantic segmentation and monocular depth estimation tasks. The experimental results, as shown in Table 3, reveal that (i) VersaViT demonstrates superior performance to SigLIP 2 on both tasks, although there remains a slight gap compared to DINOv3. (ii) In particular, our method delivers substantial improvements over the Qwen2-VL-ViT baseline. For semantic segmentation, the performance increases from 33.6 to 49.6 on ADE20k and from 67.5 to 86.6 on Pascal VOC. For monocular depth es-

timation, the RMSE on the KITTI dataset is dramatically reduced from 3.735 to 3.136, and on the NYUv2 dataset, it drops from 0.541 to 0.473. These results demonstrate that our method significantly enhances the representational quality of dense features within the vision backbone.

Table 5. Ablation study on loss weights.

λ_{cap}	λ_{depth}	λ_{seg}	OpenCompass \uparrow	NYUv2 \downarrow	ADE20k \uparrow
Baseline (Qwen2-VL-ViT)			64.8	0.541	33.6
0.50	0.25	0.25	66.5	0.470	48.3
0.25	0.50	0.25	65.7	0.455	48.9
0.25	0.25	0.50	65.7	0.476	50.0
0.33	0.33	0.33	66.4	0.473	49.6

5.3. Ablation Study & Analysis

In this section, we further investigate the effect of our method, for example, the effectiveness of multi-task training, the generalization of our method, *etc.*

Effectiveness of Multi-task Training. As shown in Table 4, it can be observed that as the number of tasks during the multi-task collaborative training phase increases, the model’s overall performance improves. The following key observations can be made: (i) Training only the VQA and Image Captioning tasks effectively enhances the model’s performance on the VQA benchmark, but it degrades the vision backbone’s dense feature representation. This finding aligns with the observation made in Section 3. (ii) Jointly training the VQA and depth tasks significantly improves the model’s performance on both VQA and depth-related tasks. (iii) Adding the segmentation task further enhances the model’s capabilities, not only improving segmentation performance but also boosting performance in both VQA and depth tasks. Collectively, integrating these three tasks results in a more comprehensive visual representation.

Ablation Study on Loss Weights. As shown in Table 5, we conduct ablation experiments under different loss-weight settings. The experimental results indicate that increasing the loss weight of a specific task generally leads to slightly improved performance on that task. Moreover, balanced weights achieve the optimal trade-off among all tasks. Importantly, our method is robust to weight variations, as all configurations significantly outperform the baseline.

Generalization on Different Vision Backbones. In this section, we investigate the application of our multi-task post-training framework across different vision backbones. As shown in Table 6, our approach is compatible with various ViT architectures and consistently enhances the performance of the backbones across multiple aspects.

Data-driven Vs. Method-driven Gains. To isolate the effect of multi-tasking from data scaling, we introduce a baseline model trained on a 35M-scale dataset using only captioning and VQA tasks, excluding the multi-tasking

Table 6. Ablation study on different vision backbones.

Model	OpenCompass \uparrow	NYUv2 \downarrow	ADE20k \uparrow
Qwen2-VL-ViT	64.8	0.541	33.6
VersaViT	66.4 (+1.6)	0.473 (-0.068)	49.6 (+16.0)
Qwen2.5-VL-ViT	64.0	0.533	37.2
VersaViT-Qwen-2.5	65.2 (+1.2)	0.464 (-0.069)	47.2 (+10.0)
Siglip2-so400M-512	59.3	0.497	40.9
VersaViT-Siglip2	60.4 (+1.1)	0.481 (-0.016)	49.2 (+8.3)

Table 7. Effectiveness of multi-tasking vs. data scaling.

Model	OpenCompass \uparrow	NYUv2 \downarrow	ADE20k \uparrow
35M-Baseline	66.2	0.547	34.7
VersaViT	66.4	0.473	49.6

Table 8. Evaluation of 3D consistency of dense representations.

Method	Geometric		Semantic	
	NAVI (Recall)	SPair (Recall)	NAVI (Recall)	SPair (Recall)
Qwen2-VL-ViT [68]	39.27		17.05	
VersaViT	41.64 (+2.37)		26.99 (+9.94)	

Table 9. Comparison of zero-shot relative depth estimation performance. Ours is trained via multi-task learning without task-specific fine-tuning. * denotes fine-tuning on the depth task.

Method	KITTI [18]		NYUv2 [56]		DA-2K [79]	
	AbsRel \downarrow	$\delta_1\uparrow$	AbsRel \downarrow	$\delta_1\uparrow$	Acc(%)	
Specialist Models						
DPT [52]	10.0	90.1	9.8	90.3	-	
MiDaS V3.1 [2]	12.7	85.0	4.8	98.0	-	
DepthFM [20]	8.9	91.3	5.5	96.3	85.8	
Marigold [28]	9.9	91.6	5.5	96.4	86.8	
Depth Anything V2 [79]	7.5	94.8	4.4	97.9	97.4	
Ours	9.4	90.5	7.7	94.4	91.3	
Ours*	7.1	94.5	5.3	96.9	94.2	

Table 10. Comparison of image referring segmentation performance. Results are shown for the fine-tuning setting (post-training on RefCOCO datasets).

Method	refCOCO [27]			refCOCO+ [27]			refCOCOg [44]		
	val	testA	testB	val	testA	testB	val(U)	test(U)	
Specialist Models									
LAVT [80]	72.7	75.8	68.8	62.1	68.4	55.1	61.2	62.1	
ReLA [35]	73.8	76.5	70.2	66.0	71.0	57.7	65.0	66.0	
LISA-7B [32]	74.1	76.5	71.1	62.4	67.4	56.5	66.4	68.5	
VISA-7B [74]	72.4	75.5	68.1	59.8	64.8	53.1	65.5	66.4	
Sa2VA-26B [84]	82.5	-	-	78.8	-	-	79.7	-	
Ours	78.8	81.2	76.2	69.4	75.0	63.9	72.0	74.3	

framework. As demonstrated in Table 7, this comparison confirms that the performance gains stem from our multi-tasking methodology rather than mere data scaling.

Enhanced 3D Correspondence. We follow the evaluation setting established by Probe3D [16] to assess geometric correspondence on the NAVI dataset [24] and semantic cor-

respondence on the SPair dataset [45]. As demonstrated in Table 8, VersaViT significantly outperforms the baseline, achieving a 2.3-point increase on NAVI and a significant 10-point increase on SPair. This compelling evidence strongly indicates that our method effectively enhances the 3D-aware representations of the vision backbone. Further details are provided in the supplementary materials.

Transfer to Tasks Learned During Multi-task Training. Through the multi-task training stage, our model naturally acquires the ability to perform monocular depth estimation and image referring segmentation. For monocular depth estimation, we evaluate our model on three benchmarks, with the results detailed in Table 9. Despite being trained solely via multi-task learning, our method achieves performance on par with that of specialized depth estimation models. Moreover, after subsequent fine-tuning specifically for the depth estimation task, our model attains performance comparable to state-of-the-art methods, demonstrating that VersaViT is highly adaptable to the depth estimation task.

Table 11. Comparison of zero-shot image-text retrieval performance. Results are evaluated under two settings: (i) fine-tuning only the projection layers, and (ii) unfreezing the vision backbone to fully exploit the retrieval potential. * denotes the second setting.

Method	COCO		Flickr	
	T \rightarrow I	I \rightarrow T	T \rightarrow I	I \rightarrow T
CLIP-L [50]	36.5	56.3	65.2	85.2
EVA-CLIP-8B [58]	53.0	70.3	80.8	95.6
SigLIP [86]	52.0	70.2	80.5	93.5
SigLIP 2 [62]	55.8	71.7	85.7	94.9
DINOv3 [57]	45.6	63.7	-	-
Aligned on 30M image-text pairs				
Ours	46.9	60.5	77.0	88.3
Ours*	54.8	69.5	82.2	92.5

Similarly, for image referring segmentation, the experimental results are shown in Table 10. After fine-tuning the multi-task pre-trained model on the RefCOCO datasets, our model substantially outperforms a wide range of specialized methods, demonstrating strong transferability.

Transfer to Retrieval Tasks. To assess the performance of our trained vision backbone on retrieval tasks, we select `siglip2-so400m-patch14-384` as the text encoder. We conduct two experimental settings: a frozen configuration, where only the vision attention pooling layer and the text projection are trained; and a more extensive setting where the vision encoder training is enabled to fully explore the potential of our model. For training data, we use the CC3M, CC12M, and YFCC15M datasets, as used in [88]. For further details regarding the data and architecture, please refer to the supplementary materials.

The experimental results, presented in Table 11, show that our model exhibits exceptional retrieval performance across various settings. Notably, with only 30M training

samples and training solely the lightweight projection layer, our model surpasses CLIP and achieves comparable performance to DINOv3. Furthermore, when the vision encoder is enabled, our model performs slightly behind SigLIP 2 by about 2 points. This outcome clearly indicates that the vision encoder trained using our framework still demonstrates strong potential and competitiveness in retrieval tasks.

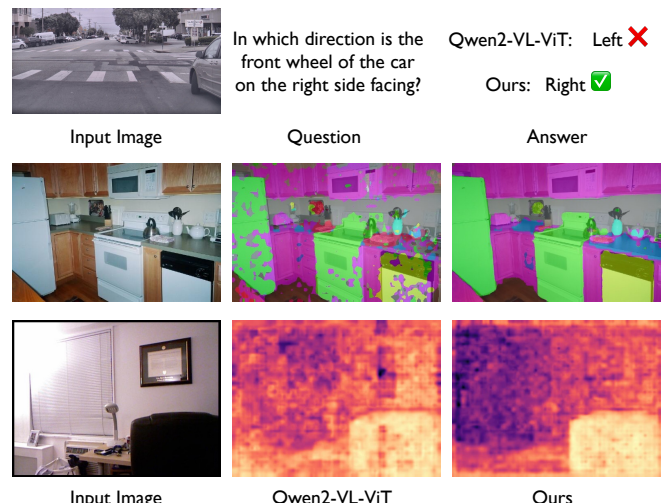


Figure 4. Qualitative examples. Qualitative comparison of VersaViT against Qwen2-VL-ViT across three tasks. For the VQA, we evaluate using Qwen3-8B. The results for semantic segmentation and depth estimation are obtained through linear probing. As shown, our method outperforms the baseline in all these tasks.

Discussion on Seamless Integration. While our multi-task collaborative training method is validated via post-training on the vision encoder, its design enables seamless integration into any stage of MLLM training (*e.g.*, pre-training, decay, and post-training). Typically, MLLM training relies exclusively on autoregressive loss; in contrast, our method augments this with two pixel-level objectives. This integration is facilitated by batch-wise task alternation, wherein only one task-specific loss is computed per batch. Such a design ensures that our method can be seamlessly adapted to existing MLLM training frameworks. Moreover, we anticipate that applying our approach during the earlier phases of MLLM training will allow the vision backbone to acquire more precise and semantically rich feature representations, which we consider an avenue for future work.

5.4. Qualitative Results

In Figure 4, we provide a qualitative comparison of VersaViT with the Qwen2-VL-ViT baseline across three tasks: VQA, semantic segmentation, and depth estimation. As demonstrated, after undergoing multi-task collaborative training, VersaViT significantly outperforms the baseline in each of these tasks. For instance, the example in the first row illustrates that our model exhibits a superior com-

hension of spatial relationships. Furthermore, the examples in the second and third rows highlight our model’s enhanced ability to capture fine-grained features, resulting in more precise object segmentation and depth estimation.

6. Conclusion

In this paper, we have identified that the vision encoders in current MLLMs exhibit deficiencies in their dense feature representations, as manifested in their suboptimal performance on dense prediction tasks. To address this issue, we proposed VersaViT, a well-rounded vision backbone that employs a multi-task collaborative post-training paradigm. Specifically, our approach simultaneously leverages three distinct tasks: VQA and image captioning, monocular depth estimation, and image referring segmentation. The collaborative training aims to adapt MLLM vision encoders to achieve superior performance on both VQA and vision-centric tasks, ultimately enabling a versatile VFM. Furthermore, extensive experiments on a wide range of downstream tasks have demonstrated the significant improvement achieved by our method. We anticipate that our framework will provide valuable insight into visual foundation models and stimulate further research in this area.

References

- [1] Shuai Bai, Kebin Chen, Xuejing Liu, Jialin Wang, Wenbin Ge, Sibo Song, Kai Dang, Peng Wang, Shijie Wang, Jun Tang, et al. Qwen2. 5-vl technical report. *arXiv preprint arXiv:2502.13923*, 2025. [1](#), [2](#), [3](#), [6](#)
- [2] Reiner Birk, Diana Wofk, and Matthias Müller. Midas v3.1-a model zoo for robust monocular relative depth estimation. *arXiv preprint arXiv:2307.14460*, 2023. [7](#)
- [3] Ali Furkan Biten, Ruben Tito, Lluis Gomez, Ernest Valveny, and Dimosthenis Karatzas. Ocr-idl: Ocr annotations for industry document library dataset. In *ECCV*, 2022. [4](#), [5](#), [13](#)
- [4] Daniel Bolya, Po-Yao Huang, Peize Sun, Jang Hyun Cho, Andrea Madotto, Chen Wei, Tengyu Ma, Jiale Zhi, Jathushan Rajasegaran, Hanoona Rasheed, et al. Perception encoder: The best visual embeddings are not at the output of the network. *arXiv preprint arXiv:2504.13181*, 2025. [6](#)
- [5] Tom Brown, Benjamin Mann, Nick Ryder, Melanie Subbiah, Jared D Kaplan, Prafulla Dhariwal, Arvind Neelakantan, Pranav Shyam, Girish Sastry, Amanda Askell, et al. Language models are few-shot learners. In *NIPS*, 2020. [2](#)
- [6] Mathilde Caron, Hugo Touvron, Ishan Misra, Hervé Jégou, Julien Mairal, Piotr Bojanowski, and Armand Joulin. Emerging properties in self-supervised vision transformers. In *ICCV*, 2021. [2](#)
- [7] Rich Caruana. Multitask learning. *Machine learning*, 1997. [2](#)
- [8] Soravit Changpinyo, Piyush Sharma, Nan Ding, and Radu Soricut. Conceptual 12m: Pushing web-scale image-text pre-training to recognize long-tail visual concepts. In *CVPR*, 2021. [5](#)
- [9] Lin Chen, Jinsong Li, Xiaoyi Dong, Pan Zhang, Conghui He, Jiaqi Wang, Feng Zhao, and Duhua Lin. Sharegpt4v: Improving large multi-modal models with better captions. In *ECCV*, 2024. [14](#)
- [10] Lin Chen, Jinsong Li, Xiaoyi Dong, Pan Zhang, Yuhang Zang, Zehui Chen, Haodong Duan, Jiaqi Wang, Yu Qiao, Duhua Lin, et al. Are we on the right way for evaluating large vision-language models? In *NIPS*, 2024. [6](#)
- [11] Mehdi Cherti, Romain Beaumont, Ross Wightman, Mitchell Wortsman, Gabriel Ilharco, Cade Gordon, Christoph Schuhmann, Ludwig Schmidt, and Jenia Jitsev. Reproducible scaling laws for contrastive language-image learning. In *CVPR*, 2023. [6](#)
- [12] Michael Crawshaw. Multi-task learning with deep neural networks: A survey. *arXiv preprint arXiv:2009.09796*, 2020. [2](#)
- [13] Matt Deitke, Christopher Clark, Sangho Lee, Rohun Tripathi, Yue Yang, Jae Sung Park, Mohammadreza Salehi, Niklas Muenninghoff, Kyle Lo, Luca Soldaini, et al. Molmo and pixmo: Open weights and open data for state-of-the-art vision-language models. In *CVPR*, 2025. [1](#), [4](#), [5](#), [13](#)
- [14] Shangzhe Di, Zhonghua Zhai, and Weidi Xie. Revisiting multi-task visual representation learning. *arXiv preprint arXiv:2601.13886*, 2026. [2](#)
- [15] Haodong Duan, Junming Yang, Yuxuan Qiao, Xinyu Fang, Lin Chen, Yuan Liu, Xiaoyi Dong, Yuhang Zang, Pan Zhang, Jiaqi Wang, et al. Vlmevalkit: An open-source toolkit for evaluating large multi-modality models. In *ACMMM*, 2024. [14](#)
- [16] Mohamed El Banani, Amit Raj, Kevis-Kokitsi Maninis, Abhishek Kar, Yuanzhen Li, Michael Rubinstein, Deqing Sun, Leonidas Guibas, Justin Johnson, and Varun Jampani. Probing the 3d awareness of visual foundation models. In *CVPR*, 2024. [7](#)
- [17] David Fan, Shengbang Tong, Jiachen Zhu, Koustuv Sinha, Zhuang Liu, Xinlei Chen, Michael Rabbat, Nicolas Ballas, Yann LeCun, Amir Bar, et al. Scaling language-free visual representation learning. *arXiv preprint arXiv:2504.01017*, 2025. [6](#)
- [18] Andreas Geiger, Philip Lenz, Christoph Stiller, and Raquel Urtasun. Vision meets robotics: The kitti dataset. *The international journal of robotics research*, 2013. [7](#)
- [19] Tianrui Guan, Fuxiao Liu, Xiyang Wu, Ruiqi Xian, Zongxia Li, Xiaoyu Liu, Xijun Wang, Lichang Chen, Furong Huang, Yaser Yacoob, et al. Hallusionbench: an advanced diagnostic suite for entangled language hallucination and visual illusion in large vision-language models. In *CVPR*, 2024. [6](#)
- [20] Ming Gui, Johannes Schusterbauer, Ulrich Prestel, Pingchuan Ma, Dmytro Kotovenko, Olga Grebenkova, Stefan Andreas Baumann, Vincent Tao Hu, and Björn Ommer. Depthfm: Fast generative monocular depth estimation with flow matching. In *AAAI*, 2025. [7](#)
- [21] Dong Guo, Faming Wu, Feida Zhu, Fuxing Leng, Guang Shi, Haobin Chen, Haoqi Fan, Jian Wang, Jianyu Jiang, Jiawei Wang, et al. Seed1. 5-vl technical report. *arXiv preprint arXiv:2505.07062*, 2025. [1](#), [2](#)

[22] Kaiming He, Xinlei Chen, Saining Xie, Yanghao Li, Piotr Dollár, and Ross Girshick. Masked autoencoders are scalable vision learners. In *CVPR*, 2022. 2, 6

[23] Greg Heinrich, Mike Ranzinger, Hongxu Yin, Yao Lu, Jan Kautz, Andrew Tao, Bryan Catanzaro, and Pavlo Molchanov. Radiov2. 5: Improved baselines for agglomerative vision foundation models. In *CVPR*, 2025. 2

[24] Varun Jampani, Kevins-Kokitsi Maninis, Andreas Engelhardt, Arjun Karpur, Karen Truong, Kyle Sargent, Stefan Popov, André Araujo, Ricardo Martin Brumalla, Kaushal Patel, et al. Navi: Category-agnostic image collections with high-quality 3d shape and pose annotations. In *NIPS*, 2023. 7

[25] Chao Jia, Yinfai Yang, Ye Xia, Yi-Ting Chen, Zarana Parekh, Hieu Pham, Quoc Le, Yun-Hsuan Sung, Zhen Li, and Tom Duerig. Scaling up visual and vision-language representation learning with noisy text supervision. In *ICML*, 2021. 2

[26] Albert Q Jiang, Alexandre Sablayrolles, Antoine Roux, Arthur Mensch, Blanche Savary, Chris Bamford, Devendra Singh Chaplot, Diego de las Casas, Emma Bou Hanna, Florian Bressand, et al. Mixtral of experts. *arXiv preprint arXiv:2401.04088*, 2024. 2

[27] Sahar Kazemzadeh, Vicente Ordonez, Mark Matten, and Tamara Berg. Referitgame: Referring to objects in photographs of natural scenes. In *EMNLP*, 2014. 7

[28] Bingxin Ke, Anton Obukhov, Shengyu Huang, Nando Metzger, Rodrigo Caye Daudt, and Konrad Schindler. Repurposing diffusion-based image generators for monocular depth estimation. In *CVPR*, 2024. 7

[29] Aniruddha Kembhavi, Mike Salvato, Eric Kolve, Minjoon Seo, Hannaneh Hajishirzi, and Ali Farhadi. A diagram is worth a dozen images. In *ECCV*, 2016. 6

[30] Alexander Kirillov, Eric Mintun, Nikhila Ravi, Hanzi Mao, Chloe Rolland, Laura Gustafson, Tete Xiao, Spencer Whitehead, Alexander C Berg, Wan-Yen Lo, et al. Segment anything. In *ICCV*, 2023. 4, 5, 13

[31] Alina Kuznetsova, Hassan Rom, Neil Alldrin, Jasper Uijlings, Ivan Krasin, Jordi Pont-Tuset, Shahab Kamali, Stefan Popov, Matteo Malloci, Alexander Kolesnikov, et al. The open images dataset v4: Unified image classification, object detection, and visual relationship detection at scale. *IJCV*, 2020. 5

[32] Xin Lai, Zhuotao Tian, Yukang Chen, Yanwei Li, Yuhui Yuan, Shu Liu, and Jiaya Jia. Lisa: Reasoning segmentation via large language model. In *CVPR*, 2024. 2, 7

[33] Zeqian Li, Shangzhe Di, Zhonghua Zhai, Weilin Huang, Yanfeng Wang, and Weidi Xie. Universal video temporal grounding with generative multi-modal large language models. In *NIPS*, 2025. 2

[34] Long Lian, Yifan Ding, Yunhao Ge, Sifei Liu, Hanzi Mao, Boyi Li, Marco Pavone, Ming-Yu Liu, Trevor Darrell, Adam Yala, and Yin Cui. Describe anything: Detailed localized image and video captioning. In *ICCV*, 2025. 5, 13

[35] Chang Liu, Henghui Ding, and Xudong Jiang. Gres: Generalized referring expression segmentation. In *CVPR*, 2023. 7

[36] Haotian Liu, Chunyuan Li, Qingyang Wu, and Yong Jae Lee. Visual instruction tuning. In *NIPS*, 2023. 4

[37] Yuliang Liu, Zhang Li, Hongliang Li, Wenwen Yu, Mingxin Huang, Dezhi Peng, Mingyu Liu, Mingrui Chen, Chunyuan Li, Lianwen Jin, et al. On the hidden mystery of ocr in large multimodal models. *arXiv preprint arXiv:2305.07895*, 2023. 6

[38] Yuan Liu, Haodong Duan, Yuanhan Zhang, Bo Li, Songyang Zhang, Wangbo Zhao, Yike Yuan, Jiaqi Wang, Conghui He, Ziwei Liu, et al. Mmbench: Is your multi-modal model an all-around player? In *ECCV*, 2024. 6

[39] Yuan Liu, Le Tian, Xiao Zhou, Xinyu Gao, Kavio Yu, Yang Yu, and Jie Zhou. Points1. 5: Building a vision-language model towards real world applications. *arXiv preprint arXiv:2412.08443*, 2024. 1

[40] Yanqing Liu, Xianhang Li, Letian Zhang, Zirui Wang, Zeyu Zheng, Yuyin Zhou, and Cihang Xie. Openvision 2: A family of generative pretrained visual encoders for multimodal learning. *arXiv preprint arXiv:2509.01644*, 2025. 2

[41] Yikun Liu, Yajie Zhang, Jiayin Cai, Xiaolong Jiang, Yao Hu, Jiangchao Yao, Yanfeng Wang, and Weidi Xie. Lamra: Large multimodal model as your advanced retrieval assistant. In *CVPR*, 2025. 2

[42] Ilya Loshchilov and Frank Hutter. Decoupled weight decay regularization. *arXiv preprint arXiv:1711.05101*, 2017. 13

[43] Pan Lu, Hritik Bansal, Tony Xia, Jiacheng Liu, Chunyuan Li, Hannaneh Hajishirzi, Hao Cheng, Kai-Wei Chang, Michel Galley, and Jianfeng Gao. Mathvista: Evaluating mathematical reasoning of foundation models in visual contexts. *arXiv preprint arXiv:2310.02255*, 2023. 6

[44] Junhua Mao, Jonathan Huang, Alexander Toshev, Oana Camburu, Alan L Yuille, and Kevin Murphy. Generation and comprehension of unambiguous object descriptions. In *CVPR*, 2016. 7

[45] Juhong Min, Jongmin Lee, Jean Ponce, and Minsu Cho. Spair-71k: A large-scale benchmark for semantic correspondence. *arXiv preprint arXiv:1908.10543*, 2019. 8

[46] Kepan Nan, Rui Xie, Penghao Zhou, Tiehan Fan, Zhenheng Yang, Zhijie Chen, Xiang Li, Jian Yang, and Ying Tai. Openvid-1m: A large-scale high-quality dataset for text-to-video generation. *arXiv preprint arXiv:2407.02371*, 2024. 13

[47] Aaron van den Oord, Yazhe Li, and Oriol Vinyals. Representation learning with contrastive predictive coding. *arXiv preprint arXiv:1807.03748*, 2018. 1, 2

[48] Maxime Oquab, Timothée Darcet, Théo Moutakanni, Huy Vo, Marc Szafraniec, Vasil Khalidov, Pierre Fernandez, Daniel Haziza, Francisco Massa, Alaaeldin El-Nouby, et al. Dinov2: Learning robust visual features without supervision. *arXiv preprint arXiv:2304.07193*, 2023. 2

[49] Zhiliang Peng, Wenhui Wang, Li Dong, Yaru Hao, Shaohan Huang, Shuming Ma, and Furu Wei. Kosmos-2: Grounding multimodal large language models to the world. *arXiv preprint arXiv:2306.14824*, 2023. 5, 13

[50] Alec Radford, Jong Wook Kim, Chris Hallacy, Aditya Ramesh, Gabriel Goh, Sandhini Agarwal, Girish Sastry, Amanda Askell, Pamela Mishkin, Jack Clark, et al. Learning transferable visual models from natural language supervision. In *ICML*, 2021. 1, 2, 8, 15

[51] Samyam Rajbhandari, Jeff Rasley, Olatunji Ruwase, and Yuxiong He. Zero: Memory optimizations toward training trillion parameter models. In *SC20: International Conference for High Performance Computing, Networking, Storage and Analysis*, 2020. 13

[52] René Ranftl, Alexey Bochkovskiy, and Vladlen Koltun. Vision transformers for dense prediction. In *ICCV*, 2021. 4, 7

[53] Mike Ranzinger, Greg Heinrich, Jan Kautz, and Pavlo Molchanov. Am-radio: Agglomerative vision foundation model reduce all domains into one. In *CVPR*, 2024. 2

[54] Christoph Schuhmann, Romain Beaumont, Richard Vencu, Cade Gordon, Ross Wightman, Mehdi Cherti, Theo Coombes, Aarush Katta, Clayton Mullis, Mitchell Wortsman, et al. Laion-5b: An open large-scale dataset for training next generation image-text models. In *NIPS*, 2022. 13

[55] Shuai Shao, Zeming Li, Tianyuan Zhang, Chao Peng, Gang Yu, Xiangyu Zhang, Jing Li, and Jian Sun. Objects365: A large-scale, high-quality dataset for object detection. In *ICCV*, 2019. 5, 13

[56] Nathan Silberman, Derek Hoiem, Pushmeet Kohli, and Rob Fergus. Indoor segmentation and support inference from rgbd images. In *ECCV*, 2012. 7

[57] Oriane Siméoni, Huy V Vo, Maximilian Seitzer, Federico Baldassarre, Maxime Oquab, Cijo Jose, Vasil Khalidov, Marc Szafraniec, Seungeun Yi, Michaël Ramamonjisoa, et al. Dinov3. *arXiv preprint arXiv:2508.10104*, 2025. 2, 5, 6, 8, 14, 15

[58] Quan Sun, Jinsheng Wang, Qiying Yu, Yufeng Cui, Fan Zhang, Xiaosong Zhang, and Xinlong Wang. Eva-clip-18b: Scaling clip to 18 billion parameters. *arXiv preprint arXiv:2402.04252*, 2024. 8, 15

[59] Kimi Team, Angang Du, Bohong Yin, Bowei Xing, Bowen Qu, Bowen Wang, Cheng Chen, Chenlin Zhang, Chenzhuang Du, Chu Wei, et al. Kimi-vl technical report. *arXiv preprint arXiv:2504.07491*, 2025. 1, 2

[60] Hugo Touvron, Thibaut Laval, Gautier Izacard, Xavier Martinet, Marie-Anne Lachaux, Timothée Lacroix, Baptiste Rozière, Naman Goyal, Eric Hambro, Faisal Azhar, et al. Llama: Open and efficient foundation language models. *arXiv preprint arXiv:2302.13971*, 2023. 2

[61] Michael Tschannen, Manoj Kumar, Andreas Steiner, Xiaohua Zhai, Neil Houlsby, and Lucas Beyer. Image captioners are scalable vision learners too. In *NIPS*, 2023. 2

[62] Michael Tschannen, Alexey Gritsenko, Xiao Wang, Muhammad Ferjad Naeem, Ibrahim Alabdulmohsin, Nikhil Parthasarathy, Talfan Evans, Lucas Beyer, Ye Xia, Basil Mustafa, et al. Siglip 2: Multilingual vision-language encoders with improved semantic understanding, localization, and dense features. *arXiv preprint arXiv:2502.14786*, 2025. 1, 6, 8, 15

[63] Simon Vandenhende, Stamatios Georgoulis, Wouter Van Gansbeke, Marc Proesmans, Dengxin Dai, and Luc Van Gool. Multi-task learning for dense prediction tasks: A survey. *TPAMI*, 2021. 2

[64] Bo Wan, Michael Tschannen, Yongqin Xian, Filip Pavetic, Ibrahim M Alabdulmohsin, Xiao Wang, André Susano Pinto, Andreas Steiner, Lucas Beyer, and Xiaohua Zhai. Locca: Visual pretraining with location-aware captioners. In *NIPS*, 2024. 2

[65] Haochen Wang, Qirui Chen, Cilin Yan, Jiayin Cai, Xiaolong Jiang, Yao Hu, Weidi Xie, and Stratis Gavves. Object-centric video question answering with visual grounding and referring. In *ICCV*, 2025. 2

[66] Haicheng Wang, Chen Ju, Weixiong Lin, Shuai Xiao, Mengting Chen, Yixuan Huang, Chang Liu, Mingshuai Yao, Jinsong Lan, Ying Chen, et al. Advancing myopia to holism: Fully contrastive language-image pre-training. In *CVPR*, 2025. 2

[67] Jianfeng Wang, Xiaowei Hu, Zhe Gan, Zhengyuan Yang, Xiyang Dai, Zicheng Liu, Yumao Lu, and Lijuan Wang. Ufo: A unified transformer for vision-language representation learning. *arXiv preprint arXiv:2111.10023*, 2021. 2

[68] Peng Wang, Shuai Bai, Sinan Tan, Shijie Wang, Zhihao Fan, Jinze Bai, Keqin Chen, Xuejing Liu, Jialin Wang, Wenbin Ge, et al. Qwen2-vl: Enhancing vision-language model's perception of the world at any resolution. *arXiv preprint arXiv:2409.12191*, 2024. 1, 2, 3, 6, 7

[69] Tobias Weyand, Andre Araujo, Bingyi Cao, and Jack Sim. Google landmarks dataset v2-a large-scale benchmark for instance-level recognition and retrieval. In *CVPR*, 2020. 5

[70] Luis Wiedmann, Orr Zohar, Amir Mahla, Xiaohan Wang, Rui Li, Thibaud Frere, Leandro von Werra, Aritra Roy Gosthipaty, and Andrés Marafioti. Finevision - open data is all you need, 2025. 5, 14

[71] Jiannan Wu, Muyan Zhong, Sen Xing, Zeqiang Lai, Zhaoyang Liu, Zhe Chen, Wenhai Wang, Xizhou Zhu, Lewei Lu, Tong Lu, et al. Visionlm v2: An end-to-end generalist multimodal large language model for hundreds of vision-language tasks. In *NIPS*, 2024. 2

[72] Zhiyu Wu, Xiaokang Chen, Zizheng Pan, Xingchao Liu, Wen Liu, Damai Dai, Huazuo Gao, Yiyang Ma, Chengyue Wu, Bingxuan Wang, et al. Deepseek-vl2: Mixture-of-experts vision-language models for advanced multimodal understanding. *arXiv preprint arXiv:2412.10302*, 2024. 6

[73] LLM-Core-Team Xiaomi. Mimo-vl technical report, 2025. 1

[74] Cilin Yan, Haochen Wang, Shilin Yan, Xiaolong Jiang, Yao Hu, Guoliang Kang, Weidi Xie, and Efstratios Gavves. Visa: Reasoning video object segmentation via large language models. In *ECCV*, 2024. 7

[75] Yibin Yan, Jilan Xu, Shangzhe Di, Yikun Liu, Yudi Shi, Qirui Chen, Zeqian Li, Yifei Huang, and Weidi Xie. Learning streaming video representation via multitask training. In *ICCV*, 2025. 2

[76] Ziang Yan, Zhilin Li, Yinan He, Chenting Wang, Kunchang Li, Xinhao Li, Xiangyu Zeng, Zilei Wang, Yali Wang, Yu Qiao, et al. Task preference optimization: Improving multimodal large language models with vision task alignment. In *CVPR*, 2025. 2

[77] Biao Yang, Bin Wen, Boyang Ding, Changyi Liu, Chenglong Chu, Chengru Song, Chongling Rao, Chuan Yi, Da Li, Dunju Zang, et al. Kwai keye-vl 1.5 technical report. *arXiv preprint arXiv:2509.01563*, 2025. 2

[78] Haolin Yang, Jiayuan Rao, Haoning Wu, and Weidi Xie. Soccermaster: A vision foundation model for soccer understanding. *arXiv preprint arXiv:2512.11016*, 2025. 2

[79] Lihe Yang, Bingyi Kang, Zilong Huang, Zhen Zhao, Xiaogang Xu, Jiashi Feng, and Hengshuang Zhao. Depth anything v2. In *NIPS*, 2024. 4, 7, 13

[80] Zhao Yang, Jiaqi Wang, Yansong Tang, Kai Chen, Hengshuang Zhao, and Philip HS Torr. Lavt: Language-aware vision transformer for referring image segmentation. In *CVPR*, 2022. 7

[81] Yuan Yao, Tianyu Yu, Ao Zhang, Chongyi Wang, Junbo Cui, Hongji Zhu, Tianchi Cai, Haoyu Li, Weilin Zhao, Zhihui He, et al. Minicpm-v: A gpt-4v level mllm on your phone. *arXiv preprint arXiv:2408.01800*, 2024. 6

[82] Weijie Yin, Dingkang Yang, Hongyuan Dong, Zijian Kang, Jiacong Wang, Xiao Liang, Chao Feng, and Jiao Ran. Sailvit: Towards robust and generalizable visual backbones for mllms via gradual feature refinement. *arXiv preprint arXiv:2507.01643*, 2025. 2

[83] Weihao Yu, Zhengyuan Yang, Linjie Li, Jianfeng Wang, Kevin Lin, Zicheng Liu, Xinchao Wang, and Lijuan Wang. Mm-vet: Evaluating large multimodal models for integrated capabilities. *arXiv preprint arXiv:2308.02490*, 2023. 6

[84] Haobo Yuan, Xiangtai Li, Tao Zhang, Zilong Huang, Shilin Xu, Shunping Ji, Yunhai Tong, Lu Qi, Jiashi Feng, and Ming-Hsuan Yang. Sa2va: Marrying sam2 with llava for dense grounded understanding of images and videos. *arXiv preprint arXiv:2501.04001*, 2025. 7

[85] Xiang Yue, Yuansheng Ni, Kai Zhang, Tianyu Zheng, Ruqi Liu, Ge Zhang, Samuel Stevens, Dongfu Jiang, Weiming Ren, Yuxuan Sun, et al. Mmmu: A massive multi-discipline multimodal understanding and reasoning benchmark for expert agi. In *CVPR*, 2024. 6

[86] Xiaohua Zhai, Basil Mustafa, Alexander Kolesnikov, and Lucas Beyer. Sigmoid loss for language image pre-training. In *ICCV*, 2023. 2, 8, 15

[87] Yanzhao Zhang, Mingxin Li, Dingkun Long, Xin Zhang, Huan Lin, Baosong Yang, Pengjun Xie, An Yang, Dayiheng Liu, Junyang Lin, et al. Qwen3 embedding: Advancing text embedding and reranking through foundation models. *arXiv preprint arXiv:2506.05176*, 2025. 5

[88] Kecheng Zheng, Yifei Zhang, Wei Wu, Fan Lu, Shuailei Ma, Xin Jin, Wei Chen, and Yujun Shen. Dreamlip: Language-image pre-training with long captions. In *ECCV*, 2024. 8, 14

[89] Bolei Zhou, Agata Lapedriza, Aditya Khosla, Aude Oliva, and Antonio Torralba. Places: A 10 million image database for scene recognition. *TPAMI*, 2017. 5

[90] Jinghao Zhou, Chen Wei, Huiyu Wang, Wei Shen, Cihang Xie, Alan Yuille, and Tao Kong. ibot: Image bert pre-training with online tokenizer. *arXiv preprint arXiv:2111.07832*, 2021. 2

[91] Weiming Zhuang, Chen Chen, Zhizhong Li, Sina Sajadmanesh, Jingtao Li, Jiabo Huang, Vikash Sehwag, Vivek Sharma, Hirotaka Shinozaki, Felan Carlo Garcia, et al. Argus: A compact and versatile foundation model for vision. In *CVPR*, 2025. 2

VersaViT: Enhancing MLLM Vision Backbones via Task-Guided Optimization

Supplementary Material

7. Details about the Loss of Depth Estimation

As outlined in Section 4.2.2 of the main paper, depth estimation is optimized by employing two distinct loss functions: a scale- and shift-invariant loss (\mathcal{L}_{ssi}) and a gradient matching loss (\mathcal{L}_{gm}). Specifically, the scale- and shift-invariant loss is defined as:

$$\mathcal{L}_{ssi} = \frac{1}{HW} \sum_{i=1}^{HW} \rho(d_i^*, d_i),$$

where ρ is the affine-invariant mean absolute error loss: $\rho(d_i^*, d_i) = |\hat{d}_i^* - \hat{d}_i|$. Here, \hat{d}_i^* and \hat{d}_i represent the scaled and shifted versions of the predicted depth (d_i^*) and the ground truth (d_i), respectively. The scaling and shifting are performed by the transformation:

$$\hat{d}_i = \frac{d_i - t(d)}{s(d)},$$

where $t(d)$ and $s(d)$ are utilized to align the prediction and the ground truth to zero translation and unit scale. These aligning factors are defined as:

$$t(d) = \text{median}(d) \quad \text{and} \quad s(d) = \frac{1}{HW} \sum_{i=1}^{HW} |d_i - t(d)|.$$

In addition to \mathcal{L}_{ssi} , the gradient matching loss (\mathcal{L}_{gm}) evaluates the difference in the depth gradients between the ground truth and the rescaled estimates across multiple scales, indexed by k . This loss is formally expressed as:

$$\mathcal{L}_{gm} = \sum_{k=1}^K \sum_{i=1}^{HW} (|s \nabla_x^k d_i - \nabla_x^k d_i^*| + |s \nabla_y^k d_i - \nabla_y^k d_i^*|).$$

Consequently, the final loss function for depth estimation is formulated as a weighted combination of these two terms:

$$\mathcal{L}_{\text{depth}} = \lambda_{ssi} \mathcal{L}_{ssi} + \lambda_{gm} \mathcal{L}_{gm},$$

where λ_{ssi} and λ_{gm} denote the weight hyperparameters that govern the contribution of each loss component.

8. More Training Details

8.1. More Implementation Details

By default, we set the loss weights as follows: $\lambda_{ssi} = 1.0$, $\lambda_{gm} = 0.5$, $\lambda_{bce} = 2.0$, and $\lambda_{dice} = 0.5$. Furthermore, the weights for the various tasks are uniformly set such that

Table 12. **Data statistics for VQA evaluation.** This table summarizes the datasets utilized in the VQA evaluation stage.

Training Stage	Data Type	Data Source	Data Size
Pre-training	Captioning OCR	Laion-5B [54], OpenVid [46] Laion-5B [54]	1.7M 0.1M
Instruction-tuning	Mixed Data	Mixed Data Source	6.6M

$\lambda_{\text{cap}} = \lambda_{\text{depth}} = \lambda_{\text{seg}} = 1/3$. We employ distinct batch sizes for the different tasks. Specifically, the batch size for the VQA and image captioning tasks is set to 8 per card, while the batch size for monocular depth estimation and image referring segmentation is set to 32. In terms of input resolution, during the training of VQA and captioning, it supports a maximum image input resolution of 896×896 . For the depth estimation and referring segmentation tasks, however, we resize the images to a fixed resolution for training. Images for the image referring segmentation task are resized to 560×560 pixels. In contrast, for monocular depth estimation, we select a resolution of 532×532 pixels, which is the closest size to the 518×518 used by Depth Anything V2 [79] while still being divisible by 28. Regarding the training data, since the dataset size varies across different tasks, we perform a resampling operation on the smaller datasets before training. This procedure ensures that all tasks are trained for the same number of optimization steps. We employ the Deepspeed Zero2 [51] and gradient checkpointing strategies, utilizing AdamW [42] optimization and selecting bf16 data precision. For linear probing in semantic segmentation, the input images are resized to 560×560 pixels. For linear probing in depth estimation, we adhere to the standard resolution specified by the corresponding dataset.

8.2. More Training Data Details

This section details the dataset used for VersaViT training. For the captioning alignment stage, we use the full Pixmo-cap dataset [13], while the IDL-WDS [3] and SA-1B-InternVL [30] datasets are randomly sampled. For the multi-task collaborative training stage, depth-related data are annotated using Depth-Anything-V2-Large [79]. For referring segmentation data, such as GRIT [49], we generate the corresponding masks using SAM [30] based on the provided box annotations. For Object365 [55], the mask annotations are also produced by SAM from the bounding boxes, and the text annotations are obtained using DAM-3B-Self-Contained [34]. The SA-1B-DAM [34] dataset is directly usable without additional pro-

cessing. For VQA and captioning data, we remove pure-text and multi-image samples from FineVision [70] dataset and retain only the single-image instances.

9. More Evaluation Details

9.1. Details about the Evaluation of VQA

The training data for the VQA evaluation is detailed in Table 12. In the first stage, we use a 1.7M dataset of image captions and OCR data to warm up the vision projection, with the learning rate set to 5e-4. In the second stage, we incorporate a diverse range of data types, including OCR, math, knowledge, and openQA, with a total dataset size of 6.6M. For this stage, the learning rate is set to 2e-5. For benchmark evaluation, we utilize the VLMEvalKit [15].

9.2. Details about the Evaluation of 3D Correspondence

We adopt the evaluation setting established by DINov3 [57]. Specifically, images are resized to a side length of 448 pixels for the NAVI dataset and 896 pixels for the SPair dataset. To measure performance, we report the correspondence recall, *i.e.* the percentage of correspondences falling within a specified distance. All reported results utilize features extracted from the final layer of the backbone.

9.3. Details about the Evaluation of Depth

As outlined in Section 5.3 of the main paper, the fine-tuning setting of depth estimation employs the same training data used in the multi-task training phase. Both the vision backbone and the DPT head are initialized with the checkpoint obtained from multi-task training. The vision backbone is optimized with a learning rate of 1e-5, whereas the remaining parameters are updated using a learning rate of 1e-4. A batch size of 32 is used per GPU, and the model is trained for 5 epochs on 128 H20 GPUs.

9.4. Details about the Evaluation of Referring Seg

The fine-tuning stage involves utilizing the RefCOCO series and COCO-Stuff datasets. The vision backbone and the segmentation head are both initialized using the multi-task trained checkpoint. During this phase, the parameters for the vision backbone and the segmentation head are unfrozen. For the text encoder, we employ LoRA for fine-tuning, setting both the LoRA alpha and rank to 8. The vision backbone is trained with a learning rate of 1e-5, while the remaining parameters utilize a learning rate of 1e-4. A batch size of 32 is used per GPU, and the model is trained for 50 epochs on 8 H20 GPUs.

9.5. Details about the Evaluation of Retrieval

Given that the Qwen2-VL-ViT lacks a CLS token, we follow the approach used in SigLIP and add an attention pooling layer at the end of the vision encoder to extract global

Table 13. Parameter statistics for various task heads.

Tasks	Components	Params.
-	Vision Backbone	644.5 M
VQA&Captioning	MLP Layer	35.0 M
Referring Segmentation	Neck & Prompt Enc. & Mask Dec.	4.8 M
Depth Estimation	DPT	37.0 M

Table 14. Linear probing results on semantic segmentation with frozen backbones under different resolutions.

Method	Res.	ADE20k	Citysc.	VOC
Qwen2-VL-ViT	448	31.4	55.5	67.5
VersaViT	448	42.3 (+10.9)	66.7 (+11.2)	81.0 (+13.5)
Qwen2-VL-ViT	560	33.6	57.6	67.5
VersaViT	560	49.6 (+16.0)	74.5 (+16.9)	86.6 (+19.1)

features. This layer is specifically designed to derive a global image feature representation and comprises a multi-head attention layer followed by an MLP. Concurrently, for the text modality, we introduce a text projection layer, which is also composed of an MLP, to map the text embeddings to the same dimensionality as the image features. We specify the final shared embedding dimension to 1280.

Regarding the training data, we follow the approach outlined in [88], utilizing the CC3M, CC12M, and YFCC15M datasets. Specifically, the training process incorporates the raw caption, shortsv caption, and longsv caption fields from these sources. Here, shortsv and longsv refer to short and long captions, respectively, synthesized using ShareGPT4V [9]. To accelerate training, the text embeddings are extracted and prepared offline before the training phase. The retrieval experiments are conducted across 128 H20 GPUs for 10 epochs, with the batch size per GPU set to 128. When only the projection layer is fine-tuned, the learning rate is set to 5e-4. When the vision backbone is made trainable, its learning rate is set to 1e-5, while the learning rate for all other parameters is set to 1e-4.

10. Summarization of Lightweight Task Head

Table 13 presents the specific parameter counts of the lightweight heads used for different tasks. As shown, the parameter sizes of the task heads are minimal compared with those of the vision backbone. This design not only allows more task-related capabilities to be integrated into the vision backbone but also helps avoid excessive computational overhead.

11. Additional Experimental Results

11.1. Ablation Study on Resolution

As shown in Table 14, we perform linear probing experiments for semantic segmentation at multiple resolutions.

The results demonstrate that our model achieves consistently and significantly higher performance than the baseline across different resolutions. Furthermore, the performance improvement increases with resolution, which may be attributed to the fact that the referring segmentation task is trained at a resolution of 560×560 .

11.2. Transfer to Classification Task

To investigate the performance of our ViT when transferred to classification tasks, we fine-tune the model on 30M samples using the same experimental setup as in the retrieval evaluation. As shown in Table 15, despite being trained on only 30M samples, our model exhibits strong performance on ImageNet. Moreover, on the more fine-grained MMVP benchmark, it also achieves competitive results. These findings indicate that our ViT retains strong discriminative capability for classification.

Table 15. Performance of zero-shot image classification.

Method	ImageNet	MMVP
	Validation	Avg.
CLIP-L [50]	75.5	20.0
EVA-CLIP-8B [58]	83.5	-
SigLIP [86]	83.2	37.0
SigLIP 2 [62]	84.1	34.8
DINOv3 [57]	82.3	-
Aligned on 30M image-text pairs		
Ours	67.9	25.9
Ours*	75.6	32.6

12. Limitation and Future Work

Considering training efficiency, we currently set the upper bound of the training resolution to 896×896 , while keeping the resolutions for the depth and segmentation tasks fixed. This configuration may cause the model to learn task-specific biases at different resolutions. In future work, we will explore applying dynamic resolutions to the depth and segmentation tasks as well. One feasible strategy is to maintain a fixed resolution with each batch while varying the resolution across batches. In addition, we plan to further expand the range of dynamic resolutions used during training to enhance the model’s generalization capability.